Earth Surface Processes and Landforms
Earth Surf. Process. Landforms **26**, 1421–1442 (2001)
DOI: 10.1002/esp.287

PORE-WATER PRESSURE EFFECTS ON THE DETACHMENT OF COHESIVE STREAMBEDS: SEEPAGE FORCES AND MATRIC SUCTION

ANDREW SIMON[1]* AND ANDREW J. C. COLLISON[2]

[1] *USDA-ARS, National Sedimentation Laboratory, Oxford, MS 38655, USA*
[2] *Department of Geography, Kings College, London WC2R 2LS, UK*

Received 17 March 2000; Revised 12 December 2000; Accepted 17 September 2001

ABSTRACT

Erosion of cohesive channel materials is not fully understood, but is assumed to occur largely as a result of hydraulic shear stress. However, field and laboratory observations of pore-water pressures in cohesive streambed materials reveal the presence of positive and negative pore-water pressure effects that may significantly affect the erosion process, as contributing and resisting forces respectively.

Measurements of pore-water pressures below cohesive streambeds in the loess area of the midwestern USA were conducted *in situ* and in undisturbed cores with a digital, miniature tensiometer. Results disclosed matric suction values in the range of 15–50 kPa in eastern Nebraska and northern Mississippi. Repetitive tests in soft materials verified a change from positive pore-water pressures in the upper 10–15 cm, to negative pore-water pressures to depths of at least 50 cm. In firm materials, the entire sampled profile was unsaturated.

Laboratory experiments were carried out in which synthetic hydrographs were imposed on undisturbed streambed cores from the same sites. Miniature tensiometers in the cores monitored the resulting pattern of pore-water pressures, and revealed upward directed seepage forces on the recessional limb of the hydrograph. Maximum calculated values of the force ranged from 10 to 275 kN for the materials and heads tested. The maximum value obtained after application and release of a 2·5 m head was 119 kN, with 275 kN after a 5·0 m head. These results were supported independently by subsequent simulations using a finite-element hydrology model coupled with a stress-deformation model.

A numerical scheme was developed to calculate the forces acting on cohesive aggregates in an idealized streambed, and to evaluate the potential for their detachment. The scheme added upward-directed seepage as an additional driving force, and matric suction as an additional resisting force, to the commonly applied factors of particle weight, fluid drag and lift force. Results demonstrate that upward-directed seepage forces of the magnitude measured in the laboratory with 5·0 m stages have the potential to detach particles larger than 10 cm in diameter without requiring fluid drag and lift forces. When added to these hydraulic forces, erosion thresholds are lowered, enabling erosion at lower hydraulic stresses.

A hypothesis for detachment of chips or blocks of cohesive bed material is proposed: (1) large (>5 m) rises in stage increase pore-water pressures or decrease matric suction dramatically in the region just below the bed surface; (2) a relatively rapid decrease in stage causing a loss of water pressure above the bed, combined with low-rates of excess pore-water pressure dissipation just below the bed surface result in steepened hydraulic gradients; and (3) a resulting net upward seepage force is great enough to contribute to detachment of cohesive bed material, or rupture the bed by exceeding the available strength and confining stress. Published in 2001 by John Wiley & Sons, Ltd.

KEY WORDS: cohesive materials; seepage forces; matric suction; liquefaction; pore-water pressure; erosion

INTRODUCTION AND PURPOSE

Thousands of miles of cohesive-bed stream channels in the midwestern USA are incised and eroding at accelerated rates owing to human disturbances imposed near the turn of the twentieth century (Simon and Rinaldi, 2000). Prediction of future channel responses and the effects of potential mitigation measures are difficult because of an incomplete knowledge of erodibility and erosion mechanisms in cohesive streams. The detachment and erosion of cohesive (silt- and clay-sized) material by gravity and/or flowing water is

* Correspondence to: A. Simon, USDA-ARS, National Sedimentation Laboratory, Oxford, MS 38655, USA.
E-mail: asimon@ars.usda.gov

controlled by a variety of physical, electrical and chemical forces. Identification of all of these forces and the role that they play in determining detachment, incipient motion and erodibility of cohesive materials is still poorly understood. The behaviour of cohesive materials in flowing water is important in estimating erosion and sedimentation in a variety of types of waterways and in the associated transport of adsorbed constituents. Subaerial behaviour of cohesive materials is important in terms of determining soil detachment and erosion from channels, upland areas (by overland flow or raindrop impact), and with regard to mass movements on hillslopes and channel banks. Studies of streambank stability in cohesive materials have led to recognition of the importance of positive and negative pore-water pressures in accurate numerical analysis of mass-wasting processes and channel widening (Casagli *et al*., 1997; Simon and Curini, 1998; Rinaldi and Casagli, 1999; Simon *et al*., 1999). Negative pore-water pressures increase the shear strength of unsaturated, cohesive materials by providing tension between particles. These studies led to the idea that positive and negative pore-water pressures may play an important role in the detachment and erosion of cohesive streambed particles or aggregates.

The need for evaluation of the erodibility of cohesive streambeds in incised channels of the midwestern USA led to initial field testing of surficial critical-shear stresses (Hanson and Simon, 2001), shear strengths and pore-water pressures beneath the surface of cohesive streambeds. This field research led to the development of a hypothesis for the detachment of aggregates from cohesive streambeds as a result of upward-directed seepage forces, which is stated below.

Pore-water pressure builds up within cohesive riverbeds during the rising limb of a flood hydrograph, as pressure is transmitted through the bed and the pore fluids. As water level falls on the receding limb of the hydrograph, bed pore-water pressure also falls. However, if beds are sufficiently impermeable, pressure equalization between pores within the bed and the water at the bed surface will not occur immediately, and upward-directed seepage will occur to eliminate the excess pore-water pressure. It is hypothesized that such forces will be greatest when permeability is lowest, and when large flood peaks decline rapidly. This possibility suggests additional erosion mechanisms for cohesive beds distinct from hydraulic shear; detachment of either individual particles or aggregates by upward-directed seepage forces, or detachment of sheets of material owing to pore-water pressure exceeding the strength of the bed and applied normal stresses ('negative', or upward acting, effective stresses).

The purpose of this paper is, therefore, to test a hypothesis of the role of upward-directed seepage forces and upward effective stresses as means of detachment of cohesive streambeds using field, laboratory and numerical-modelling analyses.

COHESIVE STREAMBEDS AND THE NATURE OF COHESIVE MATERIALS

Non-cohesive materials are often described as coarse-grained materials composed of particles greater than 62 μm that resist erosion primarily through gravitational forces. These forces are a function of the size, weight, shape and surface texture of individual and neighbouring grains. Unlike cohesive materials, particle interaction is solely mechanical and is restricted to momentum exchanges occurring from fluid drag, random collisions and the interlocking support from adjacent grains. In contrast, cohesive materials resist erosion by a complex set of characteristics related to the existence of electro-chemical bonds between individual particles. The small mass of particles (in this size range) relative to their large specific surface area (area per unit particle mass) provides a net negative electrical-surface charge on the particle that is responsible for the electro-chemical forces and bonding between particles. Oppositely charged ions (counter ions) exist in a diffused state of decreasing concentration away from the particle. It is the properties of this 'double-layer' that exert strong influences on the erodibility of cohesive material (Masch, 1968). The strength of the bonds represented by the double-layer is controlled by the forces acting between particles, which include covalent bonds, electrostatic interactions, hydrogen bonds, van der Waals forces and hydration forces. Predicting detachment of cohesive streambeds is difficult as it is hard to predict the size of aggregates that form as a result of these forces.

Notwithstanding the complexities of defining driving and resisting forces operating on cohesive streambeds, prediction of incipient motion criteria and rates of cohesive-bed erosion have been shown to be a function of various parameters of the cohesive sediment as well as the pore and free fluids surrounding the particles. Soil

characteristics that have been identified as important for determining resistance to erosion include mean particle size, percentage of clay, percentage of organic matter, clay mineralogy, bulk density, pH, sodium-adsorption ratio, cation exchange capacity and pore-fluid chemistry (Grissinger, 1966, 1982; Nichols, 1986). Additional hydrologic factors influencing erodibility include water temperature, antecedent moisture conditions, rate of wetting and pore-water pressure. Erosion of cohesive materials then becomes a matter of breaking the bonds between cohesive particles or by detaching cohesive aggregates. Because of their influence on cohesive, shear, matric suction and seepage forces, pore-water pressures are investigated in both the subaerial and subaqueous environment as one of the principle controlling variables in the erosion of cohesive materials. The erosion of cohesive materials (generally estuarine muds) has been described as occurring by one of three mechanisms: (1) floc-by-floc detachment at low values of excess shear stress by the breaking of interparticle bonds, (2) by failure along some plane below the bed surface by which 'clumps' or aggregates of material are eroded at high values of excess shear, or by (3) fluidization of the mud–water interface (Mehta *et al.*, 1989). The primary flow-induced parameter characterizing the applied erosive force is bed shear stress. Hanson and Simon (2001) addressed the first mechanism. This research addresses the second and third mechanisms in varying degrees of detail as they apply to cohesive streambeds. In addition, a fourth mechanism based on research conducted during this study is proposed. This process relies on upward-directed seepage forces and 'negative' (upward acting) effective stresses within the cohesive bed to contribute to detachment of cohesive aggregates.

As bed shear stress represents a potential hydraulic-detachment mechanism operating longitudinally along the streambed, pore-water pressure gradients (i) and resulting seepage forces (j) represent a potential detachment mechanism operating vertically upward:

$$i = (h_1 - h_2)/L \tag{1}$$

where h_1 is the head at a higher position in the bed and h_2 is the head at a lower position in the bed, and L is the vertical distance between the positions, all in metres. A convenient measure of the seepage force is the force per unit volume (j), given by (Lambe and Whitman, 1969):

$$j = i\gamma_w \tag{2}$$

where j is the seepage force per unit volume, in kN m^{-3}, γ_w is the unit weight of water, in kN m^{-3}. This seepage force occurs by frictional drag as water moves through the soil skeleton.

The resistance of cohesive materials to erosion is often not considered in terms of hydraulic resistance to particle-by-particle or floc-by-floc detachment, but by geotechnical resistance to failure along a plane or circular arc. In this case, resistance can be described in terms of a shearing resistance or shear strength. For a planar failure of unit width and length, shear strength can be represented by the Coulomb equation:

$$S_r = c' + (\sigma - \mu)\tan\phi' \tag{3}$$

where S_r is the shear strength, c' is the effective cohesion, σ is total normal stress, μ is pore-water pressure, all in kPa, and ϕ' is the effective friction angle, in degrees. The total normal stress is given by:

$$\sigma = W\cos\beta \tag{4}$$

where W is the weight of the failure block and β is the angle of the failure plane.

In saturated conditions effective normal stress is expressed as total normal stress minus pore-water pressure. If pore-water pressure exceeds total normal stress, the value of effective normal stress becomes negative, indicating that stress is acting upwards rather than downwards. In the part of a cohesive matrix above the 'normal' level of the groundwater table (phreatic surface) and capillary fringe, materials are unsaturated, pores are filled with water and with air, and pore-water pressure is negative. The difference ($\mu_a - \mu_w$) between the air pressure (μ_a) and the water pressure in the pores (μ_w) represents matric suction (ψ). The increase in

shear strength owing to an increase in matric suction is described by the angle ϕ^b. Incorporating this effect into the standard Mohr–Coulomb equation produces (Fredlund *et al.*, 1978):

$$S_r = c' + (\sigma - \mu_a)\tan\phi' + (\mu_a - \mu_w)\tan\phi^b \quad (5)$$

where S_r is the shear strength, $(\sigma - \mu_a)$ is the net normal stress on the failure plane at failure, μ_w is the pore-water pressure on the failure plane at failure, all in kPa. The value of ϕ^b generally is between 10° and 20°, with a maximum value approaching ϕ' under saturated conditions (Fredlund and Rahardjo, 1993; Simon *et al.*, 1999). The effect of matric suction on shear strength is reflected in the apparent or total cohesion (c_a) term although this does not signify that matric suction is a form of cohesion (Fredlund and Rahardjo, 1993):

$$c_a = c' + (\mu_a - \mu_w)\tan\phi^b = c' + \psi\tan\phi^b \quad (6)$$

Negative pore-water pressures, therefore, enhance cohesion and shear strength. Furthermore, because channel-bed slopes and, therefore, failure-plane angles (β) are flat (say about 0·001 m m^{-1}), the friction terms contained in Equations 5 and 6 can be neglected, leaving only c_a (Equation 6).

To investigate the effectiveness of seepage forces in detaching and entraining cohesive aggregates, an analysis of the geotechnical and hydraulic forces acting on the aggregates is performed. Dunne (1990) investigated this phenomenon in the context of a surface layer of cohesive material and indicated that failure by seepage would occur when the thickness of a surface layer (Z) was:

$$Z = c/[(i\gamma_w) - (\gamma_s - \gamma_w)(1 - p)] \quad (7)$$

where p is the soil porosity and cohesion (c) was not defined as either effective or apparent. Using this equation Montgomery (1999) found the upward seepage force ($j = i\gamma_w$) to be ineffective at entraining cohesive aggregates from a gully head. This in part could be due to (1) overestimation of cohesion (20 kPa) by assuming c_a was c', and (2) dealing only with hydrostatic pressure gradients. The analysis compares forces acting over an area with forces acting over a volume and is independent of particle size and shape. In the study described in this paper, stresses are converted to forces by multiplying by the associated area or volume. Representative values of the seepage force measured in the field and modelled numerically are combined with measured unit weight and cohesive-strength data to evaluate the effectiveness of seepage forces as a mechanism for dislodging cohesive aggregates on streambeds.

METHODS OF INVESTIGATION

In an effort to ascertain the critical conditions for detachment by upward-directed seepage forces of cohesive streambeds along several stream systems in the loess area of the midwestern USA, a field programme was initiated to measure various physical parameters related to cohesive materials. The parameters measured include particle-size distribution, bulk unit weight, moisture content, pore-water pressures (and matric suction), effective shear-strength parameters (cohesion and friction angle), and the erodibility coefficient k by which critical shear stress, τ_c, can be calculated. Partheniades (1965) suggests that the most dependable tests of the erosion flux for cohesive beds are in a naturally sedimented channel. Creating an artificial or remoulded bed with properties similar to the natural bed is a difficult, if not an impossible task. Laboratory experiments using undisturbed cores and numerical simulations of pore-water pressure distributions and the magnitude and direction of seepage forces also were undertaken in order to investigate alternative mechanisms.

Field data collected in situ

Testing of cohesive streambeds in incised channels was undertaken in western Iowa, western Tennessee, eastern Nebraska, northeastern Missouri, and northern Mississippi during several periods between November 1997 and September 1999 in materials ranging from 11 to 37 per cent clay content.

Physical characteristics. Apparent cohesion and friction-angle data were obtained from direct shear, consolidated drained tests performed on the walls of a borehole below the surface of the streambed (Luttenegger and Hallberg, 1981). A coffer dam was used to keep stream water from flowing into the hole from the bed surface. In some cases, however, the hole did fill with fluid from leakage under the coffer dam and from seepage below the bed. Borehole shear tests were generally conducted at depths between 0·2 and 0·4 m.

Pore-water pressure measurements were taken with a digital, miniature (5 mm diameter) tensiometer. This instrument is capable of attaining equilibrium readings of positive or negative pore-water pressures after being inserted into the sample for about 120 s. Readings were taken until measured pore-water pressure was relatively constant. Repetitive tests also were conducted in the same sample to assure consistency of results. Vertical pore-water pressure distributions were measured initially by inserting the tensiometer into open-face cores extracted from depths up to 0·5 m below the surface of the streambed. In many cases measured pore-water pressures were negative. To be assured that these negative values were not the result of dilation or drying caused by removal of the sample from the bed, successive tests also were conducted on core samples encased in a 5-cm-diameter aluminium sleeve, and finally, on *in situ* bed material within a small coffer dam.

Analysis of upward-directed seepage forces

To test a hypothesis of aggregate detachment by upward-directed seepage forces and upward acting effective stress, laboratory experiments on 'undisturbed cores' and numerical simulations using a finite-element seepage model (SEEP/W) and a stress-deformation model (SIGMA/W) were conducted. (Mention of trade names or commercial products in this article is solely for the purpose of providing specific information and does not imply recommendation or endorsement by the U.S. Department of Agriculture.) The approach was to evaluate the effects of transient seepage caused by the rise and fall of a streamflow hydrograph. To accomplish this, 'typical hydrographs' of varying stages were simulated. The hydrographs manifest relatively steep rising and falling limbs, representative of the straightened, incised channels studied. An experimental apparatus was constructed such that a head could be introduced atop the core and then drained off to simulate a hydrograph of given height and duration. The same hydrographs were then used in the numerical analyses.

Seepage experiments with undisturbed cores. The 5-cm-wide and 15·2-cm-long cores were collected with a 'hammer-type' sampler driven into the bed surface within a coffer dam. This minimized the introduction of surface water into the core. It is very possible that cracks (the single largest cause of experimental failure) could be introduced when driving the sampler into the bed. After the core was removed, it was sealed around the caps at each end. Loss of water during the period prior to testing will cause the core to shrink and crack, thus creating preferred pathways for water. Care was also given to the cores during test preparation. Disturbances during transportation and laboratory set-up cause deformation of the material, water movement and, potentially, the formation of cracks in the soil matrix. After the cap had been removed from the top of the core, a drilling key was slid on to ensure correct placement of the tensiometers. A small drill bit was used to create the initial holes, followed by a 0·95 cm (3/8″) bit (tensiometer cup size) to hull-out space for the tensiometer cup. The three tensiometers were then inserted into the core and sealed at the core casing with epoxy 3·5 cm from the top, 3·5 cm from the bottom, and in the middle, 4·125 cm from the top and bottom tensiometers. To ensure that there were no leakages between the head pipe and the core, a tight rubber gasket was placed around the top of the core. After sealing lubricant was added, the core was placed into the testing pipe.

For testing, the head initially was at zero and negative pore-water pressures were obtained. Head was raised to an idealized base-flow level of 43·5 cm and maintained for 1–2 h. Head was then slowly added over 1–2 h until it reached the desired head, 2·5 m or 5 m. Maximum head was reached and maintained for approximately 1–4 h. After this period, head was slowly lowered to the 43·5 cm base-flow height. This recession process generally took 2–4 h. After head was lowered, tensiometer readings were recorded for the remainder of a 24-h period. For all subsequent tests on the core, the initial head was set to 43·5 cm.

Finite-element simulations of seepage forces and effective stresses. To verify and extend the experimental results obtained with the core samples, particularly the magnitude of the seepage forces, numerical modelling was undertaken using a commercially available finite-element hydrology model SEEP/W (GeoSlope International, 1998a). Additional analysis was conducted in which SEEP/W was coupled with a finite-element

stress-deformation model SIGMA/W (GeoSlope International 1998b). SEEP/W is a two-dimensional finite element hydrology model that simulates the movement of water and the resulting pore pressures for both saturated and unsaturated conditions using Richards' equation (Richards, 1931). The governing differential equation in SEEP/W calculates movement of water into and out of an element such that:

$$\frac{\partial}{\partial x}\left(k_x \frac{\partial H}{\partial x}\right) + \frac{\partial}{\partial y}\left(k_y \frac{\partial H}{\partial y}\right) + Q = \frac{\partial \Theta}{\partial t} \tag{8}$$

where k_x is the hydraulic conductivity in the x-direction, in m s^{-1}, H is total head, in metres, k_y is the hydraulic conductivity in the y-direction, in m s^{-1}, Q is the applied boundary flux, in m^3 s^{-1}, Θ is the volumetric moisture content, in m^3 m^{-3} and t is the time, in seconds (GeoSlope International, 1998a).

All simulations were performed on an idealized riverbed based on typical field conditions for cohesive beds analysed in northern Mississippi and eastern Nebraska. The bed was 10 m wide, and simulated to a depth of 2·5 m below the surface. The lower and lateral perimeters of the bed were fixed as zero-flux boundaries. Although some seepage probably occurs through these boundaries under field conditions, it was assumed that over the course of the simulations (24 h) the amounts would be negligible compared with movement across the upper boundary. Trial simulations with different bed configurations showed these dimensions to encompass all parts of the bed that displayed dynamic pore-pressure behaviour while eliminating significant edge effects that might be an artifact of the finite-element mesh.

The first set of simulations was performed selecting a permeability and suction-moisture function from the SEEP/W function library (GeoSlope International, 1998a). The soil type was 'clayey silt' (silty clay under the U.S. Department of Agriculture soil texture classification) with a saturated conductivity of $8{\cdot}4 \times 10^{-9}$ m s^{-1} and saturated moisture content by volume of 41 per cent. These values lie within the range of field values measured in the loess area of the midwestern USA. Laboratory values obtained from extruded cores (23 samples) for saturated conductivity ranged from $5{\cdot}0 \times 10^{-10}$ to $5{\cdot}6 \times 10^{-7}$ m s^{-1} (mean $= 6{\cdot}6 \times 10^{-8}$) and from 29 to 66 per cent (mean = 50 per cent; 161 samples) for saturated moisture content. Steady-state analyses were first conducted using a 'baseflow' level of 0·45 m to obtain input values for transient (unsteady flow) analyses. Nine transient simulations were performed, to replicate and extend the laboratory-core experiments. The upper boundary condition was a dynamic head function replicating the 2·5-m and 5·0-m peak hydrographs, and introducing an additional hydrograph with a 7·5-m peak. Maximum head was maintained for periods of 65, 130 and 260 min at each level.

A second series of simulations was performed using SEEP/W coupled with SIGMA/W. The coupled simulations enable us to model the interaction of bed material and pore fluid in a more physically realistic way, and provide a convenient method of calculating the resulting stresses. In particular this analysis highlights the response of effective stress in the riverbed to imposed hydrographs. SIGMA/W is a two-dimensional finite element stress-deformation model. Stress is related to strain by the elastic modulus such that:

$$\sigma = E\varepsilon \tag{9}$$

where σ is the stress, in kPa, E is the elastic modulus, in kPa and ε is the strain, in m.

When coupled with SEEP/W it performs 'consolidation' type simulations in which the stresses and resulting strains of material are calculated based on the geotechnical properties of the bed and the movement of pore water. In coupled simulations, SIGMA/W calculates stresses and strains, while SEEP/W calculates pore-water pressure and routes water based on the pressure gradient, the permeability of the materials involved and the boundary conditions. Hydrographs can be simulated in SIGMA/W as dynamic fluid loads applied to the upper boundary of the bed. The coupled modelling scheme has been validated for such analyses (Wong *et al*., 1998). The lower edge of the finite-element mesh was fixed as a zero deformation boundary in all directions, whereas the lateral edges were fixed in the horizontal direction but permitted to deform vertically if appropriate. Nine scenarios were modelled using the same hydrographs as for the SEEP/W simulations, with additional simulations being performed to assess the sensitivity of the modelled bed to changes in permeability and geotechnical properties. For all simulations a linear elastic stress–strain model was selected in which

strain is proportional to stress, with the first nine simulations having an elastic modulus of 30 000 kPa, and a Poisson's ratio of 0·35. Obtaining values for elastic modulus and Poisson's ratio of bed material is highly problematic, and we have used typical values for silty clay obtained from literature (Head, 1986). It is probable that in reality most cohesive bed materials have elastic–plastic rather than linear elastic behaviour. However, given the small stresses relative to elastic modulus for these scenarios, deformation is likely to remain in the elastic portion of the stress–strain curve.

Subsequent simulations were performed using the same geotechnical properties but varying permeability across the range of values measured in the field, and holding permeability to a typical field value while varying elastic modulus across a range of possible literature values.

RESULTS OF FIELD TESTS

The average and median values of apparent cohesion (c_a; sum of effective cohesion and cohesion due to matric suction) for all tests are 8·6 and 6·0 kPa, respectively. Average and median values of c' are 3·7 and 2·0 kPa, respectively, indicating that a large proportion of the cohesive strength of these materials is due to matric suction. Friction angles ranged from 6·2° to 33·4°, with an average of 16·7°. The observation that bed shear strength as measured by standard laboratory tests (direct shear for example) do not correlate well with the derived values of critical shear stress for cohesive beds (Partheniades, 1965) may be related, in part, to lack of acknowledgement of negative pore-water pressures below the surface of the cohesive streambeds.

The widespread observation of negative pore-water pressure in cohesive-bed streams is a novel and contentious finding. Results disclosed that matric suction (ψ; negative pore-water pressure) values were as great as 15–20 kPa in eastern Nebraska and 40–60 kPa in northern Mississippi. Repetitive tests in soft, loess, or loess-derived materials verified a change from positive pore-water pressures in the upper 10–15 cm, to negative pore-water pressures to depths of at least 50 cm (Figure 1). In firmer materials such as the Porters Creek Clay Formation of West Tennessee and northern Mississippi and the DeForest Formation of western Iowa and eastern Nebraska (Bettis, 1995), the entire sampled profile was unsaturated. The average degree of saturation of these materials was about 73 per cent and coincides with an average moisture content of about 29 per cent by weight. The existence of negative pore-water pressures below the surface of these cohesive streambeds is hypothesized on the basis that cohesive streambeds in incised channels must represent overconsolidated sediments that have been subjected to greater normal stresses in the past. Pressure release and stress deformation of the material near the surface (within 0·5 m) would cause dilation (expansion), an increase in volume

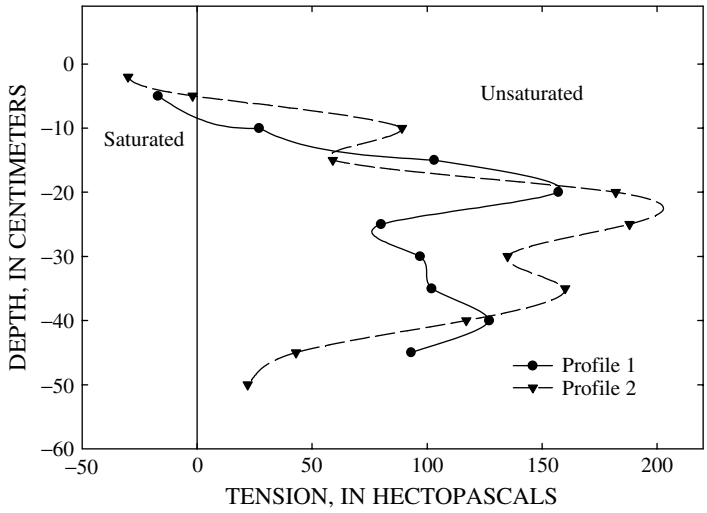

Figure 1. Distribution of pore-water pressures below the surface of cohesive streambeds in eastern Nebraska

with a commensurate decrease in bulk density and moisture content. This finding is in general agreement with the relatively low dry unit-weights obtained from core sampling (10·5–15·4 kN m^{-3}; mean = 12·8 kN m^{-3}). However, the cohesive matrix would still inhibit infiltration owing to its very low permeability (in the order of 10^{-9} to 10^{-10} m s^{-1}). The movement of water to and through these beds has been observed to occur along preferential flow along paths of weakness such as fractures, bedding planes, decayed root cavities and bioturbated pathways. We hypothesize that areas of the bed between such pathways, therefore, remain unsaturated. 'Normal' flow levels exert only small pressures on the streambed, thereby minimizing infiltration into the bed matrix. Surface seals also may contribute to the phenomenon.

That cohesive streambeds can be unsaturated and, therefore, display matric suction indicates that resistance to erosion of aggregates is enhanced by the tension provided within the cohesive matrix. If we assume an angle of 15° for ϕ^b (approximate average reported in Fredlund and Rahardjo, 1993), given that the average matric suction values measured within the upper 0·5 m are about 20 kPa, average increases in apparent cohesion of about 6 kPa owing to matric suction are possible.

Results of core experiments

Sixty tests were performed on cores obtained between 1997 and 1999 from the midwestern USA. Tests were considered 'good' if the middle and lower tensiometers did not display evidence of instantaneous response with the application of head. Simultaneous response of all tensiometers at the application of head was the result of cracks within the core formed during sampling, handling, or from desiccation during storage. Twenty tests (12 with heads of 5·0 m; 8 with heads of 2·5 m) were considered good, in that tensiometer response was delayed as the pressure front moved into the core. Each of the good tests displayed negative pore-water pressures during simulated base flow. All but five of the good tests developed an upward-directed pore-pressure gradient (i; negative value) and seepage force (j; negative value) on the falling limb of the hydrograph.

Example results are shown for a 2·5-m head applied to a core taken from West Tarkio Creek, Iowa (Figure 2). The lags associated with infiltration of water and the application of pressure to peak values within the core are shown in Figure 2a through the first 4 h of testing. Upon removal of the applied head (hydrograph recession) pressure dissipated initially in the area closest to the surface of the core (0 to 3·5 cm). Dissipation of pore-water pressure below 3·5 cm lagged behind creating a greater pore-water pressure at depth and an upward-directed seepage force. In this case, a maximum upward-directed seepage force of about 140 kN m^{-3} occurred about 4 h into the test in the upper 3·5 cm (Figure 2b). This was the time when the deepest tensiometer (number 3) was recording peak values of pore-water pressure from the initial application of head. The duration of this seepage force, although attenuated with time, was about 6·5 h (Figure 2b). Upward-directed seepage forces subsequently were generated between the deeper tensiometers.

Maximum values of the upward-directed seepage force that were generated on the recessional limb in the cores ranged from 10 to 275 kN. The maximum value obtained after application of the 2·5-m head was 119 kN; 275 kN after the 5·0-m head. The magnitude of this upward-directed seepage force indicates that it may play an important role in detaching cohesive aggregates from the streambed, once we consider the types of resisting forces. Table I provides a summary of the results from the core experiments at heads of 2·5 and 5·0 m. The average, maximum upward-seepage force was about 37 to 51 kN m^{-3} for the 5·0-m tests and about 20 to 25 kN m^{-3} for the 2·5-m tests.

Results of seepage force simulations

Results of numerical simulations show upward-directed seepage forces in the range of those measured experimentally under 2·5- and 5·0 m heads. The maximum upward-directed seepage forces developed on the recessional limb of simulated hydrographs following a 1-h peak were 58, 117 and 171 kN m^{-3} for the 2·5, 5·0 and 7·5 m heads, respectively. Even greater values were simulated for peaks with 2- and 4-h durations (Figure 3). As a representative example, we look at the 5·0 m, 2-h peak duration simulation. The simulated hydrograph and the pore-water pressure distribution expressed in terms of head (in metres) are shown at the end of the application of the peak stage (Figure 4). Head at the simulated bed surface was 7·5 m and decreased with depth to a hydrostatic pressure distribution and a head of 2·9 m at a depth of about 1·0 m

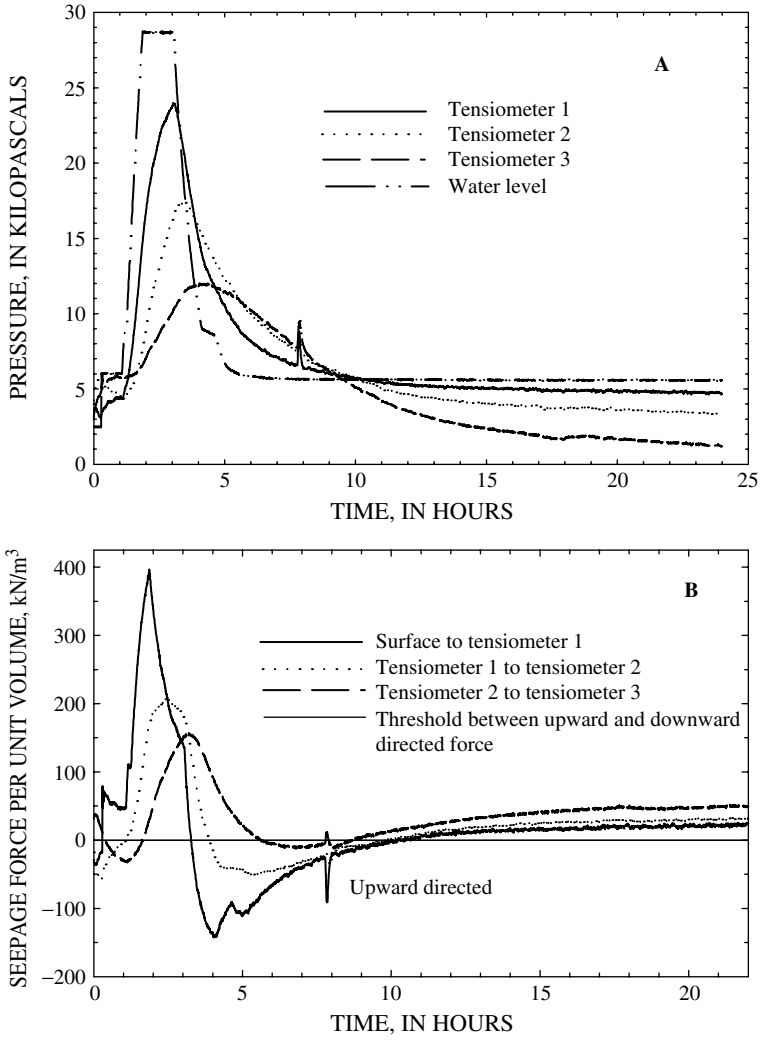

Figure 2. Example results from a test core taken from West Tarkio Creek, western Iowa showing temporal changes in pore-water pressure distributions (A), and associated temporal changes in seepage force per unit volume (B). Note that negative values of the seepage force per unit volume represent upward-directed seepage

below the surface. As with the core experiments, upward-directed seepage forces were generated on the recessional limb of the simulated hydrograph within the uppermost 0·5 m. In the example shown a peak head of 4·9 m occurred at 7 h about 0·2 m below the bed surface, decreasing rapidly towards the surface indicating a relatively steep seepage gradient and an upward-directed seepage force of 189 kN m^{-3} within the upper 0·2 m. By 9 h, the peak head decreased to 3·9 m and migrated deeper into the simulated streambed as pore-water pressures began to dissipate (Figure 4). Upward-directed seepage forces occurred down to 0·5 m below the bed surface although at a lesser magnitude.

EFFECTIVENESS OF PORE-WATER PRESSURE TO DETACH COHESIVE MATERIAL

The results of the core experiments and numerical simulations confirm the existence of relatively strong upward-directed seepage forces beneath the sampled and simulated cohesive streambeds. Using an approach similar to Engelund and Hansen (1967) for cohesionless particles, three principal forces were considered

Table I. Summary of data from core experiments

Sample location	Test number	Initial head (cm)	Time head raised (h)	Maximum head (m)	Duration rising (h)	Duration peak (h)	Duration falling (h)	Test duration (h)	Maximum or minimum pressure gradient (kPa m^{-1})				Average (kPa)
									T1 : T3	T2 : T3	T1 : T2	H_2O : T1	
Wehrspahn Creek tributary	1	0·0	2·50	5·0	1·88	1·86	4·33	17·77	−49·2	129·0	−461·6	−15·4	−116·0
Wehrspahn Creek tributary	2	43·5	0·50	5·0	2·44	1·52	3·25	24	−24·7	18·6	−114·6	−31·3	−42·4
Little Silver Creek	1	0·0	3·26	5·0	1·50	1·00	8·27	23·79	−27·9	−26·8	−30·7	−8·9	−22·1
West Tarkio Creek	1	0·0	5·75	5·0	1·74	1·05	11·58	21·93	−11·9	−165·6	−19·5	−123·1	−102·7
Haines Branch	1	0·0	3·25	5·0	1·30	0·50	4·85	24	−30·1	−45·4	−24·5	−29·3	−33·1
Haines Branch	3	43·5	3·20	5·0	2·93	2·35	5·2	24	11·0	10·0	10·4	9·9	10·1
Haines Branch	4	43·5	0·86	5·0	0·70	3·80	3·46	24	−46·0	−38·4	−56·0	−46·6	−47·0
Big Creek number 6	3	43·5	0·84	5·0	0·80	1·37	6·49	19·5	99·5	80·3	113·7	113·3	102·4
Buck Creek	1	0·0	2·25	5·0	1·42	1·38	3·2	17·5	151·1	165·7	134·3	−135·1	55·0
Buck Creek	3	43·5	2·00	5·0	1·50	1·12	3·23	24	85·4	−136·1	−11·9	−275·7	−141·2
Beal Slough	2	43·5	1·00	5·0	4·00	2·00	8	24	−7·9	−86·0	54·11	−16·1	−16·0
Mean gradient for 5·0 m head									13·6	−8·6	−36·9	−50·8	−32·1
West Tarkio Creek	2	0·0	1·00	2·5	0·86	1·09	3	24	−25·1	−9·3	−50·4	−119·0	−59·6
Wehrspahn Creek tributary	1	0·0	3·95	2·5	2·00	1·00	2·43	24	−41·1	−80·49	−17·7	−45·3	−47·8
Little Silver Creek	2	43·5	1·16	2·5	1·3	1·00	4·12	24	−38·6	−39·35	−38·6	−13·7	−30·6
Haines Branch	2	0·0	1·50	2·5	0·84	1·00	4·8	24	−15·0	11·5	16·9	9·3	12·6
Big Creek number 6	1	0·0	4·66	2·5	2·00	0·94	2·23	24	69·2	39·77	99·4	208·0	115·7
Buck Creek	2	43·5	1·02	2·5	0·76	0·97	4·27	24	47·2	−39·06	115·9	−107·4	−10·2
Beal Slough	1	0·0	3·33	2·5	1·33	1·00	7	24	27·8	9·91	44·0	27·1	27·0
W. Papillon at Blondo	1	0·0	3·00	2·5	1·86	1·46	4·5	24	−26·4	−96·52	−4·0	−19·5	−40·0
Mean gradient for 2·5 m head									−0·26	−25·44	20·7	−7·6	−4·1

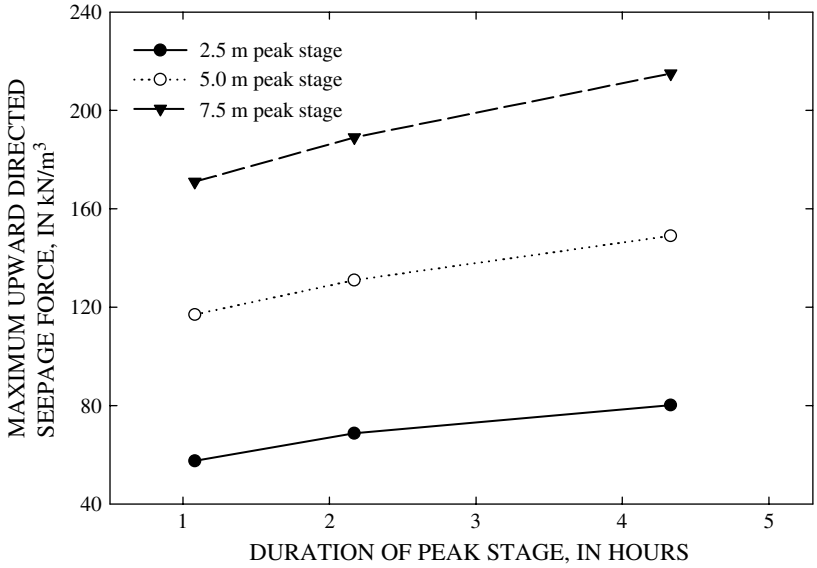

Figure 3. Range of upward-directed seepage forces generated by numerical simulations for varying peak stages and durations

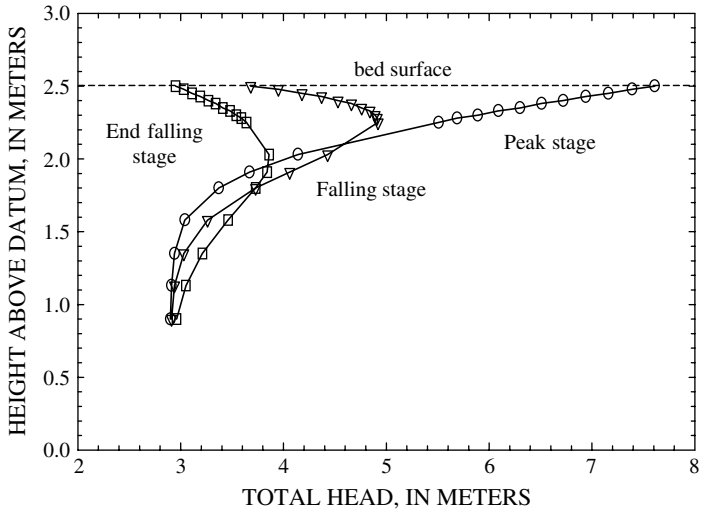

Figure 4. Example results of numerical simulations of pore-water pressure distributions (expressed as total head, in metres) for the case of a 5·0 m, 2-h peak at the end of application of peak stage, during recession and following recession

acting on the streambed particles: the submerged weight of the particle acting downward, the drag force acting downstream, and an upward-directed lift force (Dingman, 1984). In the analysis described here, two additional forces that are germane to cohesive materials were added. Cohesion acts with the particle weight to resist detachment while the upward-directed seepage force acts with the drag and lift forces to enhance detachment. Consider now a cohesive streambed as a uniform, semi-infinite medium composed of packed, spherical particles. For the purposes of this specific case, one half of a single particle was assumed to protrude above the bed surface and into the water column. Fluid drag and lift forces acting on the particle initially were ignored in order to elucidate the effects of seepage forces on the particle (Figure 5a). The forces resisting detachment (F_R) of the particle were made up of the submerged unit weight ($\gamma_t - \gamma_w$) of particle diameter

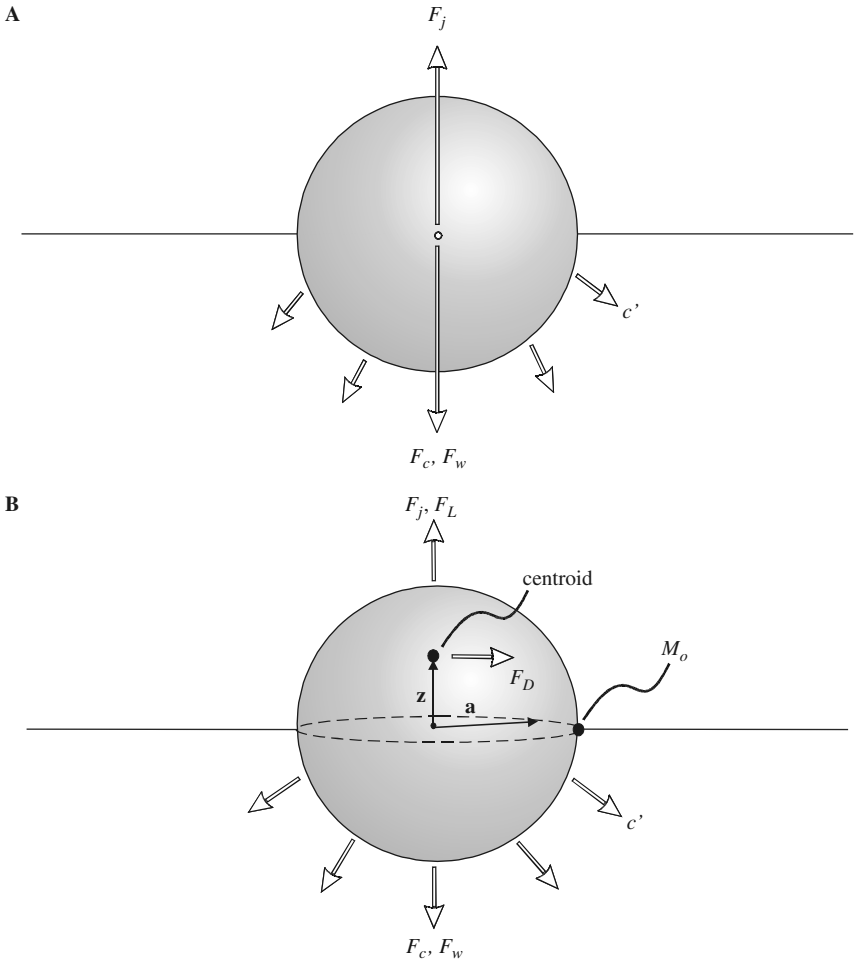

Figure 5. Schematic of conceptualized force distribution around a cohesive aggregate considering only seepage and other vertical forces (A) and including hydraulic drag and lift forces as a moment balance (B): F_j, seepage force; c', effective cohesion; F_c, cohesion force; F_w, weight force; F_L, lift force; F_D, drag force; z, height of exposed hemisphere centroid; a, radius of aggregate; M_0, turning point

d, acting over its volume and the effective cohesion (c') acting over the surface area of the sphere extending below the bed surface (F_c). Thus, the downward force due to the particle's weight is (F_w)

$$F_w = (\gamma_t - \gamma_w)4/3\pi(d/2)^3 \tag{10}$$

and the force due to cohesion is

$$F_c = c'2\pi(d/2)^2 \tag{11}$$

In this initial case, the driving (or detachment) force (F_E) was composed only of the upward-directed seepage force per unit volume (j) acting over the volume of the particle. The upward-directed seepage force (F_j) is given as

$$F_j = i\gamma_w 4/3\pi(d/2)^3 \tag{12}$$

Starting from the general condition of equilibrium (sum of moments) we derive the following erosion threshold. Expressing all forces in consistent units (in this case kN) as a force balance, provides a dimensionless quantity

representing an erosion threshold due to seepage forces (E_{tj}):

$$E_{tj} = F_R/F_E = (F_w + F_c)/F_j \tag{13}$$

Detachment by seepage forces is indicated when $E_{tj} < 1{\cdot}0$.

To include the effect of hydraulic forces acting on the protruding portion of the particle we consider the drag force:

$$F_D = C_D 0{\cdot}5\pi(d/2)^2(\rho/2)V_0^2 = C_D 0{\cdot}5\pi(d/2)^2(\rho/2)(1/n)^2(y^{4/3})S \tag{14}$$

where F_D is the drag force, in N, C_D is the drag coefficient (assumed here to be 0·4 for a submerged particle in turbulent flow (Rouse, 1937)), ρ is the density of water (1000 kg m^{-3}), V_0 is the bed velocity in m s^{-1}, n is Manning's roughness coefficient (assumed to be 0·02), y is flow depth (assumed to be 1·0 m), and S is the energy slope (assumed to be 0·003). Assumed hydraulic variables are representative of average conditions in the streams studied. The assumed 1·0-m flow depth was a reasonable estimate of depths during flow recession. Lift forces (F_L) were taken to be equal to one half the drag force (Vanoni, 1975, p. 104), particularly for the relatively smooth beds studied here. An erosion threshold, however, can no longer be calculated in terms of a simple force balance but must be analysed as a force moment balance because the drag force operates normal to the other forces described. To accomplish this we again define our spherical particle protruding above the bed surface but now add a centre of rotation ('pivot point'; M_0) at the downstream end of the particle where it intersects the bed surface (Figure 5b). First moments with respect to the pivot point are a function of the radius of the particle (a) and its centroid (z). The centroid's position for a hemisphere protruding above the bed surface becomes (C. Alonso, USDA-ARS National Sedimentation Laboratory, personal communication, 2000):

$$z = (3/8)a \tag{15}$$

The drag torque becomes the product of F_D and z, and all of the other forces are multiplied by a to obtain the balance of moments about the centre of rotation (M_0). An erosion threshold is thus defined as:

$$\Sigma M = zF_D + aF_L + aF_j - aF_c - aF_w \tag{16}$$

where the condition $\Sigma M > 0$ indicates that the particle will be dislodged. Computations for all forces represented in Equations 10–16 are carried out for the following data ranges: d from 2 μm to 0·2 m, c' from 1·0 to 20 kPa, and j from 50 to 300 kN m^{-3}. Results of the numerical analysis are summarized in Figure 6 for varying j and a constant c' of 3·75 kPa, and in Figure 7 for varying c' with a constant j of 125 kN m^{-3}. Aggregates of various diameters that exceed detachment thresholds for given combinations of seepage and cohesion values are shown shaded in grey.

Aggregate detachment is more likely with increasing seepage force and decreasing cohesion (Figures 6 and 7). The very large values of the detachment threshold considering only seepage as the driving force (E_{tj}) are because at small diameters cohesive strength applied over the surface area is much greater than the seepage applied over the volume of the particle. As particle diameter increases this difference becomes smaller and then reverses, indicating detachment, as the upward-directed seepage force exceeds aggregate resistance (Figures 6 and 7). By accounting for fluid drag (F_D), detachment-threshold values (E_t) are reduced for a given particle diameter, cohesive strength, and seepage force, indicating a greater likelihood of detachment. The effects of fluid drag on E_t are large at small aggregate diameters because aggregate weight (F_w) is very small relative to F_D. With increasing diameter this effect is reduced because F_w increases faster than F_D does.

Upward-directed seepage forces generated during transient-flow conditions in a cohesive streambed can be effective at contributing to detachment of cohesive aggregates, particularly if combined with the drag and lift forces provided by streamflow. Data show that the smallest particles within a continuous bed that could be dislodged by upward-directed seepage forces acting alone generally are in the range of 2 to 10 cm (Figure 6). This is shown to occur at seepage forces per unit volume greater than or equal to 125 kN m^{-3} at the default

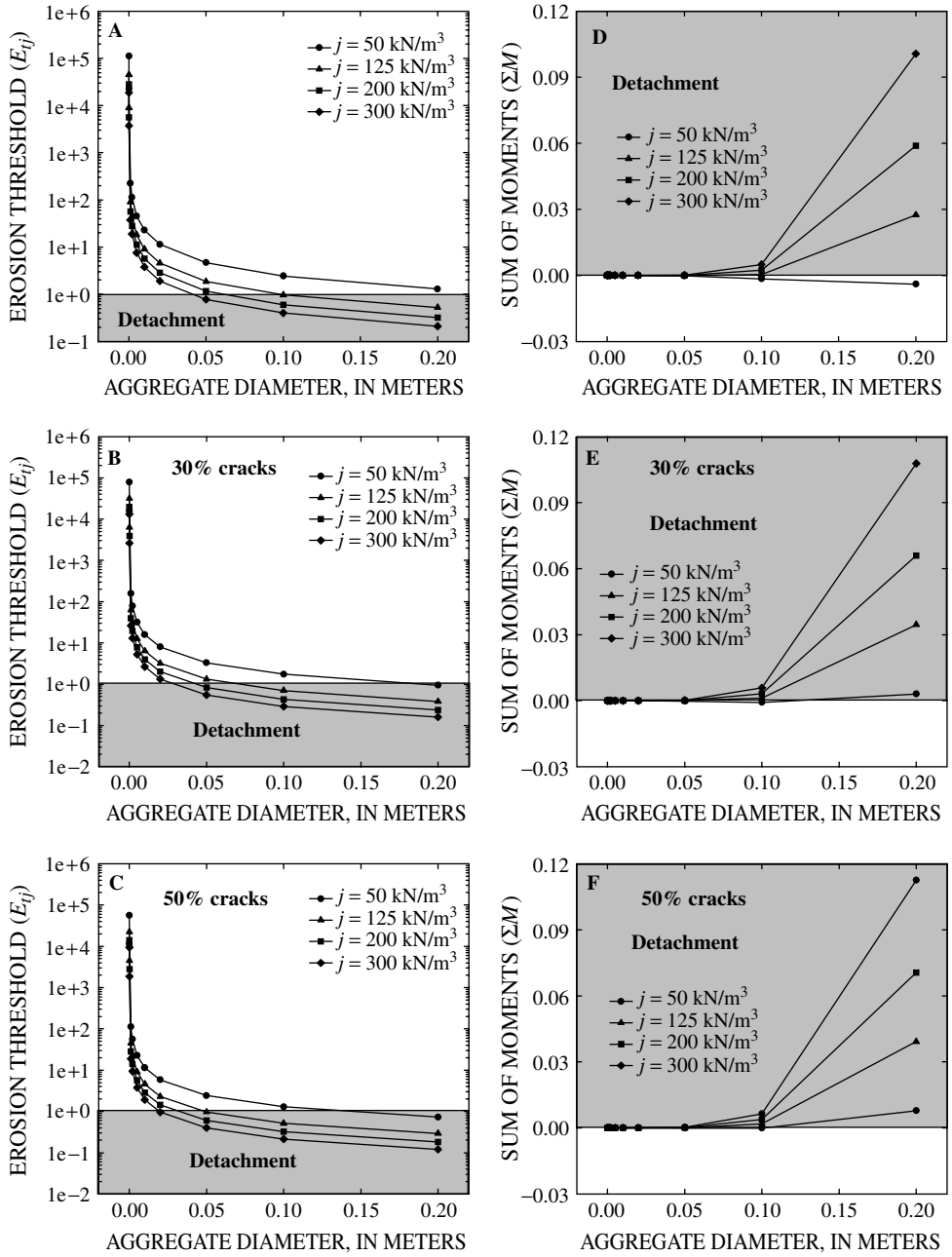

Figure 6. Erosion threshold values for varying amounts of seepage force per unit volume and particle diameter showing effects of seepage forces only (E_{tj}) and seepage, drag and lift forces (ΣM). Shaded area represents conditions for erosion. Effective cohesion = 3·75 kPa

effective cohesion of 3·75 kPa. For the smallest particles analysed, the fluid drag force is small (in the range of 10^{-12} to 10^{-11} kN), yet because it is five orders of magnitude greater than the normal force its inclusion results in a drastic reduction in E_t values. Still, the cohesive force is sufficient to resist detachment by the combined driving forces. The relative effect of fluid drag on E_t is reduced with increasing particle diameter because the submerged unit weight increases faster than does the force due to fluid drag. Smaller particles can be entrained by only moderate upward-directed seepage forces (125 kN m^{-3}) if effective cohesion is

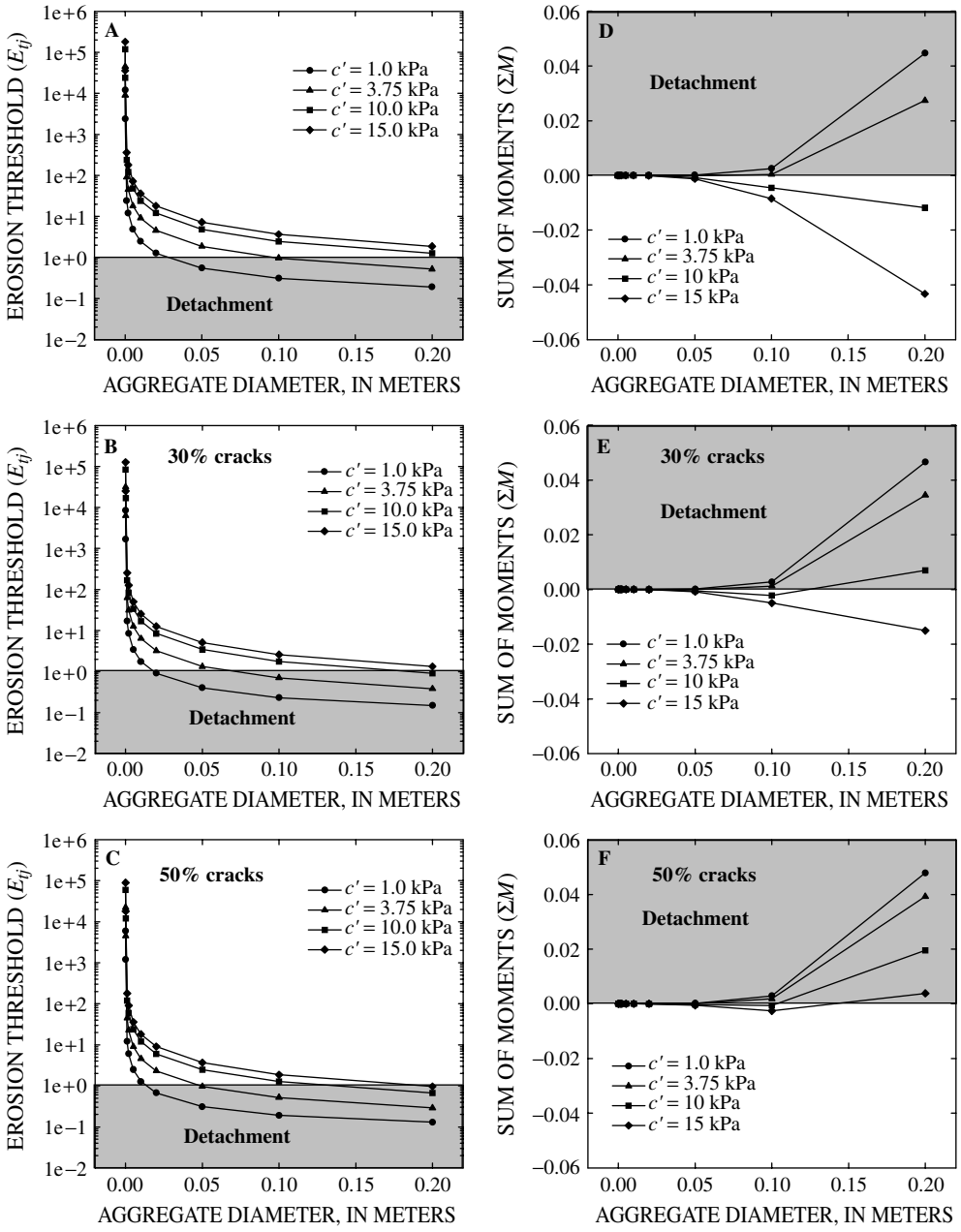

Figure 7. Erosion threshold values for varying amounts of effective cohesion and particle diameter showing effects of seepage forces only (E_{tj}) and seepage, drag and lift forces (ΣM). Shaded area represents conditions for erosion. Seepage force (j) = 125 kN m^{-3}

less than 2·5 kPa (Figure 7). For greater values of j, detachment by seepage forces may be applicable for aggregates ranging from 0·5 to 20 cm.

The dominant force resisting dislodgement by seepage forces is cohesion, representing the strength of the interparticle bonds. The cohesive force exceeds the resistance provided by the normal force by one to six orders of magnitude (for the default cohesion of 3·75 kPa) as particle size decreases from 20 cm to 2 μm. It is the resistance to detachment provided by cohesion operating over the contact surface area of the particle that

makes these materials more difficult to entrain than cohesionless particles of the same size. Cohesive forces greater than between 5 to 10 kPa are sufficient to resist dislodgment of cohesive aggregates at the default *j*-value of 125 kN m^{-3} unless additional factors or forces are considered. Greater seepage forces, representing the maximum values measured in the cores, are sufficient to dislodge 5–20 cm particles (Figure 7). The factors that might lead to an increased likelihood of erosion by seepage forces include a reduction in cohesive forces by the loss of contact surface area because of cracks, forces operating within submerged cracks or planes of weakness within the streambed, and a quasi-liquefaction of surface layers as a result of seepage forces. The latter factor is addressed in greater detail in the following section.

Field observations in the midwestern USA confirm that cohesive streambeds erode in aggregates or chips and that these chips become rounded by abrasion during subsequent transport. These chips fail along bedding planes and fractures. Many of these streambeds become partially exposed during low-flow periods, resulting in cracking by drying, freeze–thaw effects, peeling and spalling of surface layers and the formation of dessication cracks. Irrespective of the genesis of the cracks, planes of weakness are created where the cohesive aggregates have lost contact. This results in a loss in the cohesive force (F_c) because the contact surface area is reduced.

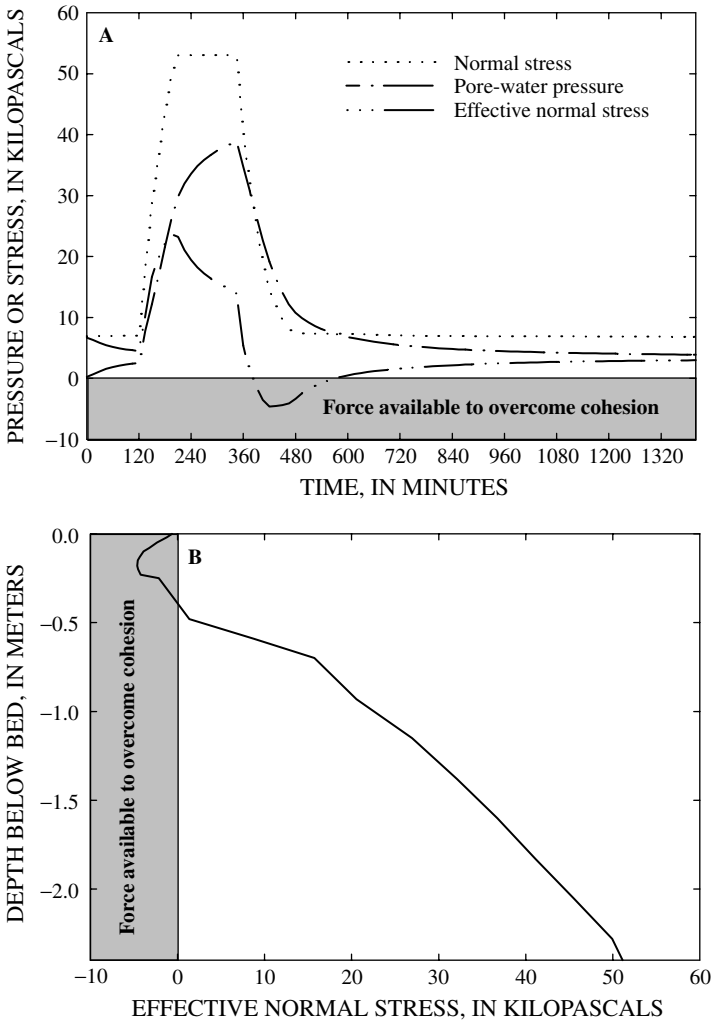

Figure 8. Example of coupled SEEP/W and SIGMA/W model results for the case of a 5·0 m peak stage and peak duration of 130 min (A), and distribution of effective normal stress with depth on the recessional limb of the streamflow hydrograph (B)

To test this effect, the contact surface area was reduced by 30% and 50% and E_{tj} and E_t were recalculated. The effect of the simulated cracks was to lower the cohesive resistance of the material. The results indicate that over the range of j and c', cracks or planes of weakness on the streambed can cause a sufficient reduction in the cohesive force to cause particles as small as 5 mm to become dislodged (at $c' = 1{\cdot}0$ kPa). A much more common occurrence, however, was that larger aggregates such as 5-cm particles were readily detached. Upward-directed seepage forces less than 100 kN m^{-3}, such as those generated by flows less than 2·5 m deep, however, were generally ineffective at dislodging cohesive aggregates (Figure 6). The same was true for streambeds with cohesions greater than about 10 kPa (Figure 7).

Our analysis uses submerged unit weight, on the assumption that the entire aggregate is surrounded by water. For the lower half of the aggregate this implies that it is surrounded by water-filled, connected pores. Field observations (Figure 1) support this assumption for aggregates that occupy the upper 10 cm of a cohesive bed, but suggest that below this aggregates may intrude into a zone that is unsaturated for some or all of the flood duration. For these aggregates we would expect effective unit weight to be higher, as not all the aggregate is surrounded by water. This would increase the force resisting detachment. In addition, such aggregates would have increased apparent cohesion due to matric suction, further increasing resistance. Predicting which aggregates would be affected in this way requires modelling of wetting front depths during flow events, which is beyond the scope of this paper. However, the observations suggest that aggregates greater than 10–20 cm in diameter will begin to be affected in this way, imposing an upper limit on the size of aggregate detached by seepage forces. This implies that the detachment curves in figures 6 and 7 will trend back towards non-detachment for aggregates larger than this size.

Results of effective stress simulations

To offer further parallel support to the thesis that upward-directed seepage forces can be effective at dislodging cohesive aggregates and cause liquefaction to a fluidized state, additional finite-element computer simulations were performed on idealized riverbeds using coupled hydrology and stress-deformation modelling (SEEP/W and SIGMA/W).

Results of coupled SEEP/SIGMA modelling were again in broad agreement with those found in the laboratory-core experiments. Output (Figure 8a) shows pore-water pressure within the bed rising in response to a 5·0 m peak-flow stage, but with a lag as a result of the relative impermeability of the bed. As stage fell, pore pressure responded but, again, with a lag. During the falling limb of the hydrograph pore-water pressure temporarily exceeded the combined normal stress imposed by the weight of water in the channel and of the bed, and effective stress acted upward (negative values). Upward effective stress occurred, in this example, at depths between 0·0 and 0·45 m (Figure 8b).

The set of nine hydrograph simulations shows a strong relationship between both flood peak and peak duration, and effective stress (Figure 9 and Table II). In every case pore pressure exceeded normal stress and effective stress acted upwards at some stage during the simulation. This state was reached on the falling limb of the streamflow hydrograph, at a time when normal stress due to the high stage had been released but pore-water pressure within the bed had yet to equilibrate (Figure 8a). Typically this state was found approximately 1 h after the peak flow had started to recede. The magnitude of the upward effective stress ranged between 0·47 and 10·8 kPa. Characteristic strengths for cohesive beds measured in northern Mississippi and the midwestern USA are approximately 4 to 8 kPa, indicating that during events with peaks greater than 5·0 m, sheets or flakes of bed material could detach owing to pore-water pressure exceeding strength and confining pressure. At lower flows where upward effective stress is less than cohesion, the upward pressure is assumed to reduce the critical shear stress required for detachment. The depth at which the minimum effective stress occurred varies from 7·5 to 22·5 cm (Table II), suggesting that significant volumes of bed material could be eroded in this way. The results also suggest that the rate at which a hydrograph falls is as important as its magnitude. Additional simulations in which the rate of hydrograph recession was decreased showed that upward effective stress still occurred, but that the magnitude was reduced.

The model results show that pore-water pressures can significantly exceed normal stress on the recessional limb of the hydrograph. As cohesive streambeds frequently have cohesion values in the same range, these

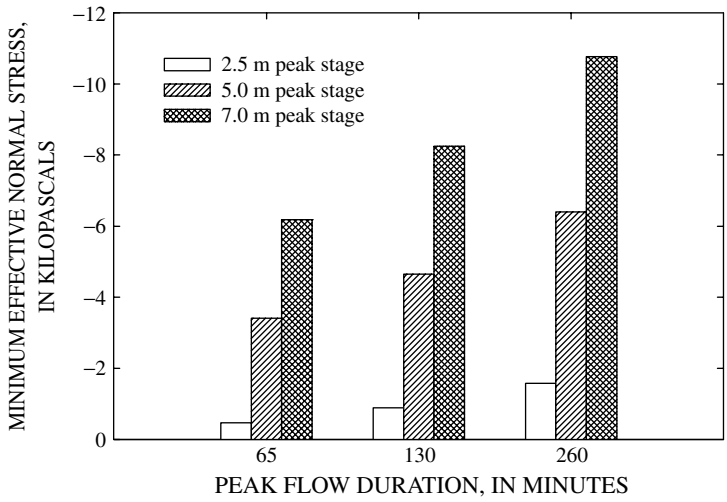

Figure 9. Maximum upward effective normal stress for the nine coupled SEEP/W and SIGMA/W simulations

Table II. Summary input and output of nine coupled SEEP/W and SIGMA/W simulations

Duration of peak (min)	Height of peak (m)	Min. effective stress σ'_{min} (kPa)	Depth of σ'_{min} (cm)	Time of σ'_{min} (minutes after peak recedes)
65	2·5	−0·47	7·5	57
65	5·0	−3·41	15·0	82
65	7·5	−6·18	17·5	83
130	2·5	−0·89	10·0	67
130	5·0	−4·65	17·5	77
130	7·5	−8·25	20·0	78
260	2·5	−1·58	12·5	57
260	5·0	−6·40	20·0	82
260	7·5	−10·77	22·5	83

findings imply that sufficient pore-water pressure may be available to either rupture the bed by failure of chips of material or to partially liquefy the upper part of the bed and expose it to tractive stresses. Field evidence supports both processes on the recessional limb of streamflow hydrographs.

Sensitivity to hydraulic conductivity and elastic modulus. Trial simulations showed that the magnitude of maximum upward effective stress was highly sensitive to permeability and elastic modulus, but relatively insensitive to Poisson's ratio. To explore this further two sensitivity analyses were performed. In the first, hydraulic conductivity was varied between 1×10^{-9} and 5×10^{-7} m s^{-1}, which lies within the range of values measured in the field. The geotechnical properties were kept constant from the previous experiment, with an elastic modulus of 30 000 kPa and a Poisson's ratio of 0·35. The boundary condition was a 5·0-m-high peak flow sustained for 130 min. The results of the sensitivity analysis (Figure 10a) suggest that the build-up of high upward effective stresses requires low bed permeability, with more permeable beds allowing excess pressure to dissipate more rapidly. The relationship is highly non-linear, with a sharp increase in pressure build-up as permeability falls below 4×10^{-8} m s^{-1} for the conditions simulated. Beds with permeability greater than 5×10^{-7} m s^{-1} were able to dissipate pore-water pressure in step with the falling flood stage, and did not experience upward effective stress conditions.

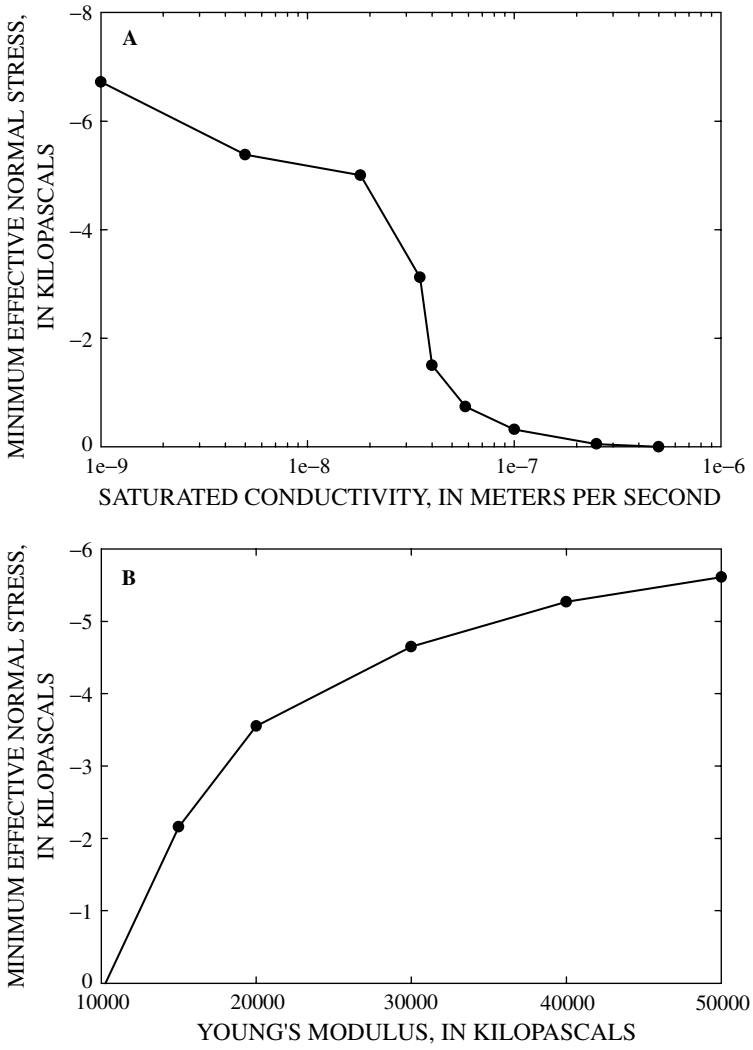

Figure 10. Sensitivity analysis for saturated hydraulic conductivity (A) and Young's modulus (B)

A second sensitivity analysis was carried out to assess the effect of elastic modulus on effective stress. Hydrologic conditions were identical to those of the initial nine simulations, with a bed hydraulic conductivity of $8{\cdot}4 \times 10^{-9}$ m s^{-1}. Poisson's ratio was 0·35. As with the first sensitivity analysis, the 5·0-m high, 130-min peak flood was used as a boundary condition. Elastic modulus was varied between 10 000 and 50 000 kPa, based on literature values for materials likely to be encountered in a cohesive bed channel (Head, 1986). The resulting simulations (Figure 10b) show a strong positive correlation between elastic modulus and peak upward effective stress, with great sensitivity between 10 000 and 30 000 kPa, and somewhat less sensitivity above this value. The results suggest that rigid beds are able to maintain large pressure differentials between the bed pore fluid and the river flow, whereas less rigid beds dissipate the pressure by skeletal expansion rather than pore seepage.

Static liquefaction or quick condition

A similar conceptual framework also can be used to investigate the effectiveness of upward-directed seepage forces in causing static liquefaction in cohesive streambeds. Static liquefaction of cohesionless materials occurs

Table III. Potential for static liquefaction of cohesive streambeds assuming $c' = 3{\cdot}75$ kPa. Note values of z and $z_c > 1{\cdot}0$ indicate liquefaction

Upward-directed seepage force (j) (kN m^{-3})	Aggregate diameter (m)	z	z_c
50	2×10^{-6}	6·11	~0·0
50	0·02	6·11	0·26
50	0·05	6·11	0·6
50	0·2	6·11	1·86
100	2×10^{-6}	12·21	~0·0
100	0·02	12·21	0·51
100	0·05	12·21	1·2
100	0·2	12·21	3·71
150	2×10^{-6}	18·32	~0·0
150	0·02	18·32	0·77
150	0·05	18·32	1·8
150	0·2	18·32	5·57

when the effective normal stress is zero. This also can be expressed as a dimensionless threshold (z) (Iverson and Major, 1986):

$$z = (i\gamma_w)/(\gamma_t - \gamma_w) \tag{17}$$

True liquefaction of materials that have cohesion is doubtful because, by definition, a total loss of strength cannot take place (Iverson and Major, 1986). However, strong upward-directed seepage forces may increase the distance between cohesive particles, resulting in weakened particle bonds (cohesion) and a 'supersaturated' or almost fluidized state. Scott (1963, p. 97) acknowledges that a critical hydraulic gradient within a cohesive soil eventually would cause a quick condition during transient flow if maintained long enough. A modification of Equation 17 that includes cohesion and a length-scaling factor (d) is proposed to investigate the conditions under which this state might occur (where $z_c \geq 1{\cdot}00$):

$$z_c = (i\gamma_w)/[(\gamma_t - \gamma_w) + c'/d] \tag{18}$$

Table III shows results for varying seepage forces and aggregate diameters using the default (average) c' value of 3·75 kPa, for c in Equation 18. As one would expect, without any cohesion the seepage forces shown (50 to 150 kN m^{-3}) are sufficient to cause liquefaction (z_c) regardless of aggregate diameter. By considering cohesion, however (z_c), Equation 18 indicates that the fluidized state envisioned by Scott (1963) and others can occur, particularly at seepage forces greater than 100 kN m^{-3}. This in fact may be quite common insofar as j values of this magnitude relate to peak stages greater than only 2·5 m in the cases tested here. These results provide an explanation for the supersaturated state encountered at shallow depths below the cohesive streambeds in eastern Nebraska and western Iowa. Subsequent flows of relatively low hydraulic shear stresses over such beds would then be capable of eroding these fluidized materials as suggested by Mehta (1991).

SUMMARY AND CONCLUSIONS

Positive and negative pore-water pressures and seepage forces have been found to play an important role in the detachment of cohesive sediments in incised stream channels. Numerical simulations and field and laboratory experiments of cohesive streambeds provide lines of parallel evidence. Erosion of cohesive streambeds is controlled partly by the magnitude and distribution of positive and negative pore-water pressures. Upward-directed

seepage forces within cohesive streambeds provide a mechanism for detaching aggregates of flocculated particles. In contrast, suction caused by negative pore-water pressures increases the cohesive strength of unsaturated cohesive streambed materials.

Measurements of pore-water pressures below cohesive streambeds in the loess area of the midwestern USA were conducted *in situ* or in undisturbed cores with a digital, miniature tensiometer. Results disclosed matric suction values as great as 15–20 kPa in eastern Nebraska and 40–50 kPa in northern Mississippi. Repetitive tests in soft materials verified a change from positive pore-water pressures in the upper 10–15 cm, to negative pore-water pressures to depths of at least 50 cm. In firm materials, the entire profile was unsaturated. Negative pore-water pressures below the surface of a cohesive streambed are explained on the basis that cohesive streambeds in incised channels must represent overconsolidated sediments where the matrix expansion results in a decrease in bulk density and moisture content. 'Normal' flow levels exert only small pressures on the streambed, thereby minimizing infiltration into the bed matrix. In addition, finite-element modelling of stress deformation indicates the possible expansion of the matrix with a consequent decrease in unit weight. This is in general agreement with the relatively low average unit-weight values obtained from core samples (dry – 12·7 kN m^{-3}; ambient – 16·9 kN m^{-3}). Upward-directed effective stresses as great as 10·8 kPa following a 4-h-long peak at a stage of 7·5 m were obtained with numerical modelling.

By accounting for resisting forces such as particle weight, cohesion and matric suction, and driving forces such as fluid drag and upward-directed seepage forces during the recessional limb of stormflow hydrographs, a numerical scheme for evaluating the potential for erosion of cohesive aggregates is obtained. Seepage forces within the cohesive streambeds are simulated numerically with finite-element software and tested via laboratory experiments using cores of cohesive streambed material for flows of 2·5, 5·0 and 7·5 m and peak durations of 1, 2 and 4 h. Maximum experimental values of the vertically upward seepage force on the recessional limb in the cores ranged from 10 to 275 kN. The maximum value obtained after application of the 2·5-m head was 119 kN; 275 kN after the 5·0-m head. Results of numerical simulations show upward-directed seepage forces in the range of those measured experimentally under 2·5 and 5·0 m heads. The maximum upward-directed seepage forces developed on the recessional limb of simulated hydrographs following a 1-h peak were 58, 117 and 171 kN for the 2·5, 5·0 and 7·5 m heads, respectively. Greater values were simulated for peaks with 2- and 4-h durations.

The model results suggest that significant upward pressure and upward ('negative') effective stress can develop in cohesive beds on the recessional limb of streamflow hydrographs. Development of upward effective stresses greater than typical bed cohesive strengths is indicated for a wide range of conditions that occur relatively frequently in streams in throughout the loess area of the midwestern USA. The frequency of such conditions, and the thickness of material affected by the processes, suggests that upward-directed seepage forces and effective stress may be significant processes in the erosion of cohesive beds. However, this mechanism requires relatively high elastic modulus and very low permeability. Beds with these properties tend to be relatively resistant to fluvial erosion, and often form hard sills or knick points in eroding beds. It could be hypothesized therefore that detachment of material from beds by pore pressure effects represents a potential erosion mechanism for 'hard' cohesive beds, whereas detachment by hydraulic shear stress represents the dominant erosion process for 'soft' cohesive beds.

ACKNOWLEDGEMENTS

We would like to express our sincere gratitude to Carlos Alonso and Eddy Langendoen, and Andrea Curini, USDA-ARS National Sedimentation Laboratory for thoughtful consultations during the initial conceptualization of the research programme and for conducting the SEEP/W simulations, respectively. We also would like to thank Mike Church and two anonymous reviewers, whose comments and criticisms of an earlier draft led to a much improved manuscript.

REFERENCES

Bett'is EA, III. 1995. *The Holocene stratigraphic record of entrenched stream systems in thick loess regions of the Mississippi River Basin*. PhD dissertation, University of Iowa: 149 pp.

Casagli N, Curini A, Gargini A, Rinaldi M, Simon A. 1997. Effects of pore pressure on the stability of streambanks: preliminary results from the Sieve River, Italy. In *Management of Landscapes Disturbed by Channel Incision*, Wang SSY, Langendoen EJ, Shields FD, Jr (eds). University of Mississippi, Oxford, Mississippi, 243–248.
Dingman SL. 1984. *Fluvial Hydrology*. WH Freeman and Company: New York; 383 pp.
Dunne T. 1990. Hydrology, mechanics and geomorphic implications of erosion by subsurface flow. In *Groundwater Geomorphology*, Higgens CG, Coates DR (eds). *Geological Society of America, Special Paper* **252**: 1–28.
Engelund F, Hansen E. 1967. *A Monograph on Sediment Transport in Alluvial Streams*. Danish Technical Press (Teknisk Forlag): Copenhagen, 62 pp.
Fredlund DG, Rahardjo H. 1993. *Soil Mechanics of Unsaturated Soils*. Wiley: New York; 517 pp.
Fredlund DG, Morgenstern NR, Widger RA. 1978. The shear strength of unsaturated soils. *Canadian Geotechnical Journal* **15**: 313–321.
GeoSlope International Ltd. 1998a. *SEEP/W Users Guide Version 4*. GeoSlope International: Calgary.
GeoSlope International Ltd. 1998b. *SIGMA/W Users Guide Version 4*. GeoSlope International: Calgary.
Grissinger EH. 1966. Resistance of selected clay systems to erosion by water. *Water Resources Research* **2**: 131–138.
Grissinger EH. 1982. Bank erosion of cohesive materials. In *Gravel-bed Rivers, Fluvial processes, Engineering and Management*, Hey RD, Bathurst JC, Thorne CR (eds). Wiley: Chichester; 273–287.
Hanson GJ, Simon A. 2001. Erodibility of cohesive streambeds in the loess area of the midwestern USA. *Hydrological Processes* **15**: 23–38.
Head KH. 1986. *Manual of Soil Laboratory Testing,* Vol. 3 *Effective Stress Tests*. Pentech Press: London.
Iverson RM, Major JJ. 1986. Groundwater seepage vectors and the potential for hillslope failure and debris flow mobilization. *Water Resources Research* **22**: 1543–1548.
Lambe TW, Whitman RV. 1969. *Soil Mechanics*. Wiley: New York; 553 pp.
Luttenegger JA, Hallberg BR. 1981. Borehole shear test in geotechnical investigations. *American Society for Testing and Materials, Special Publication* **740**: 566–578.
Masch FD. 1968. Erosion of cohesive sediments: Task Committee on Erosion of Cohesive Materials. *American Society of Civil Engineers, Journal of the Hydraulics Division* **94**: 1017–1049.
Mehta AJ. 1991. Review notes on cohesive sediment erosion. In *Coastal Sediment '91*, Kraus NC, Gingerich KJ, Kriebel DL (eds). American Society of Civil Engineers: New York; 40–53.
Mehta AJ, Hayter EJ, Parker WR. 1989. Cohesive sediment transport I: process description. *Journal of Hydraulic Engineering* **115**: 1076–93.
Montgomery DR. 1999. Erosional processes at an abrupt channel head: implications for channel entrenchment and discontinuous gully formation. In *Incised River Channels: Processes, Forms, Engineering and Management*, Darby SE, Simon A (eds). Wiley: Chichester; 247–276.
Nichols MM. 1986. Effects of fine sediment resuspension in estuaries. In *Estuarine Cohesive Sediment Dynamics, Lecture Notes on Coastal and Estuarine Studies*, Vol. 14, Mehta AJ (ed.). Springer-Verlag: Berlin.
Partheniades E. 1965. Erosion and deposition of cohesive soils. *American Society of Civil Engineers, Journal of the Hydraulics Division* **91**: 105–139.
Richards LA. 1931. Capillary conductance of liquids in porous mediums. *Physics* **1**: 318–333.
Rinaldi M, Casagli N. 1999. Stability of streambanks in partially saturated soils and effects of negative pore water pressures: the Sieve River (Italy). *Geomorphology* **26**: 253–277.
Rouse H. 1937. Modern conceptions of the mechanics of fluid turbulence. *Transactions of the American Society of Civil Engineers* **102**: 463–543.
Scott RF. 1963. *Principles of Soil Mechanics*. Addison-Wesley: Reading, MA; 550 pp.
Simon A, Curini A. 1998. Pore pressure and bank stability: the influence of matric suction. In *Hydraulic Engineering '98*, Abt S (ed.). American Society of Civil Engineers: New York; 353–363.
Simon A, Rinaldi M. 2000. Channel instability in the loess area of the midwestern United States. *Journal of the American Water Resources Association* **36**: 133–150.
Simon A, Curini A, Darby SE, Langendoen EJ. 1999. Streambank mechanics and the role of bank and near-bank processes in incised channels. In *Incised River Channels: Processes, Forms, Engineering and Management*, Darby SE, Simon A (eds). Wiley: Chichester; 123–152.
Vanoni V (ed.). 1974. *Sedimentation Engineering*. American Society of Civil Engineers: New York; 745 pp.
Wong T, Fredlund TDG, Krahn J. 1998. A numerical study of coupled consolidation in unsaturated soils. *Canadian Geotechnical Journal* **35**: 926–937.